Optics Communications 316 (2014) 228–235

Contents lists available at ScienceDirect

Optics Communications

journal homepage: www.elsevier.com/locate/optcom

Modeling the carbon nanofiber addressed liquid crystal microlens array from experimentally observed optical phenomena

Jiahui Lu *, Matthew T. Cole [1], Timothy D. Wilkinson [2]

Centre of Molecular Materials for Photonics and Electronics, Department of Engineering (Division B), University of Cambridge, CAPE Building, 9 J.J. Thomson Avenue, Cambridge CB3 0FA, United Kingdom

ARTICLE INFO

Article history:
Received 31 August 2013
Accepted 27 September 2013
Available online 4 November 2013

Keywords:
Modeling
Liquid crystal
Carbon nanofiber
Microlens
Ray tracing
Adaptive optics

ABSTRACT

This paper presents a novel method of using experimentally observed optical phenomena to reverse-engineer a model of the carbon nanofiber-addressed liquid crystal microlens array (C-MLA) using Zemax. It presents the first images of the optical profile for the C-MLA along the optic axis. The first working optical models of the C-MLA have been developed by matching the simulation results to the experimental results. This approach bypasses the need to know the exact carbon nanofiber–liquid crystal interaction and can be easily adapted to other systems where the nature of an optical device is unknown.

Results show that the C-MLA behaves like a simple lensing system at 0.060–0.276 V/μm. In this lensing mode the C-MLA is successfully modeled as a reflective convex lens array intersecting with a flat reflective plane. The C-MLA at these field strengths exhibits characteristics of mostly spherical or low order aspheric arrays, with some aspects of high power aspherics. It also exhibits properties associated with varying lens apertures and strengths, which concur with previously theorized models based on *E*-field patterns. This work uniquely provides evidence demonstrating an apparent "rippling" of the liquid crystal texture at low field strengths, which were successfully reproduced using rippled Gaussian-like lens profiles.

1. Introduction

Optical lens-like elements formed by liquid crystals (LC) when addressed with carbon nanofiber (CNF) arrays under an applied ac voltage were first reported by Wilkinson et al. in 2007 [1]. Such devices have great potential as micro-optic elements in adaptive lensing applications such as wavefront sensing, three-dimensional displays and optical tweezers [2]. Although much work has been done recently on CNF and carbon nanotube LC based electro-optic devices [3–8], the precise internal structure and CNF–LC interaction within this device under an applied voltage are considered complex and remain largely unknown.

Attempts to model the device to date have been limited to finite-element methods (FEM). This approach is labor-intensive and time consuming. So far the electric-field distribution emitted by the CNF array has been successfully modeled in this way by Butt et al. [9]. However the introduction of LC molecules grossly increases the complexity of the system and makes modeling even a single lensing element impractical. In contrast, the method presented in this paper is comparably simple, yet powerful.

Herein we report on the optical profile of the carbon nanofiber-addressed liquid crystal microlens array (C-MLA) along the optic axis under varying *E*-field strengths. To the best of our knowledge this is the first study of its kind.

Optical modeling of these phenomena is essential for developing these devices into real-world applications in optical instrumentation and design. To this end, these experiments have been simulated using Zemax [10] and we present the first models that have been developed to reproduce the experimentally observed optical phenomena. This approach bypassed the need to know the exact CNF–LC interaction and allowed us to effectively reverse-engineer a working optical model of the C-MLA in Zemax. Our simulation results matched well with experimental results and this method has proven to be a promising and useful way of characterizing several key optical phenomena exhibited by the C-MLA. Zemax is the most popular industry standard optical and illumination design software in the world and the fastest ray-tracing software in the market [11]. It offers true freedom in taking the C-MLA to the next stage in their development in a myriad of applications. Furthermore, this approach can be easily adapted to other systems where the nature of an optical device is unknown.

* Corresponding author. Tel.: +44 1223 748365.
E-mail addresses: jl424@cam.ac.uk, jiahui_lu@hotmail.com, jiahui.lu1010@gmail.com (J. Lu), mtc35@cam.ac.uk (M.T. Cole), tdw13@cam.ac.uk (T.D. Wilkinson).
[1] Tel.: +44 1223 748304; fax: +44 1223 748342.
[2] Tel.: +44 1223 748353.

0030-4018/$ - see front matter © 2014 Published by Elsevier B.V.
http://dx.doi.org/10.1016/j.optcom.2013.09.064

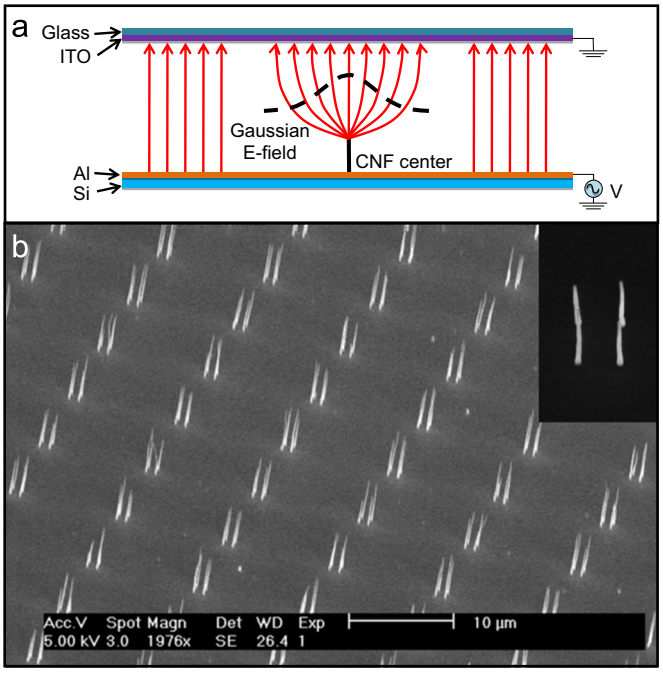

Fig. 1. Schematic of a carbon nanofiber-addressed liquid crystal microlens array (C-MLA) and scanning electron micrograph of a fabricated CNF array.

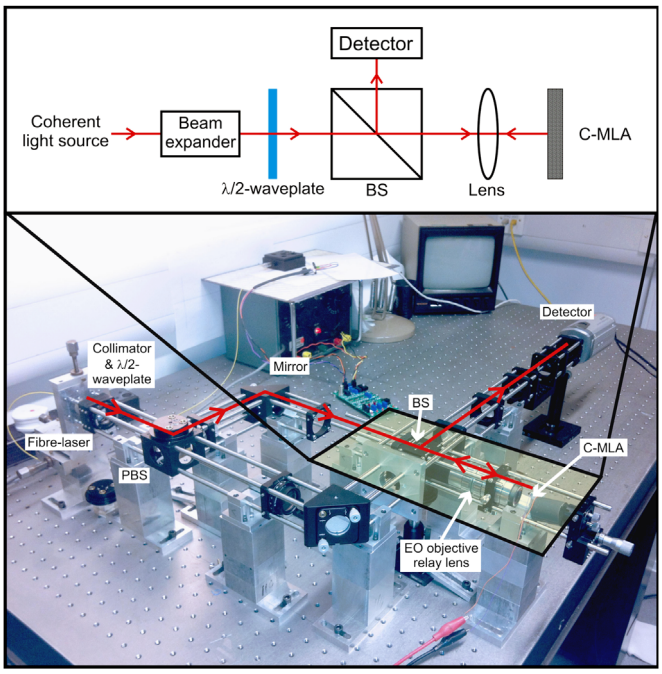

Fig. 2. Schematic layout and photograph of the experimental setup for imaging the C-MLA device [P, polarizer; BS, beamsplitter cube; PBS, polarizing beam-splitter cube].

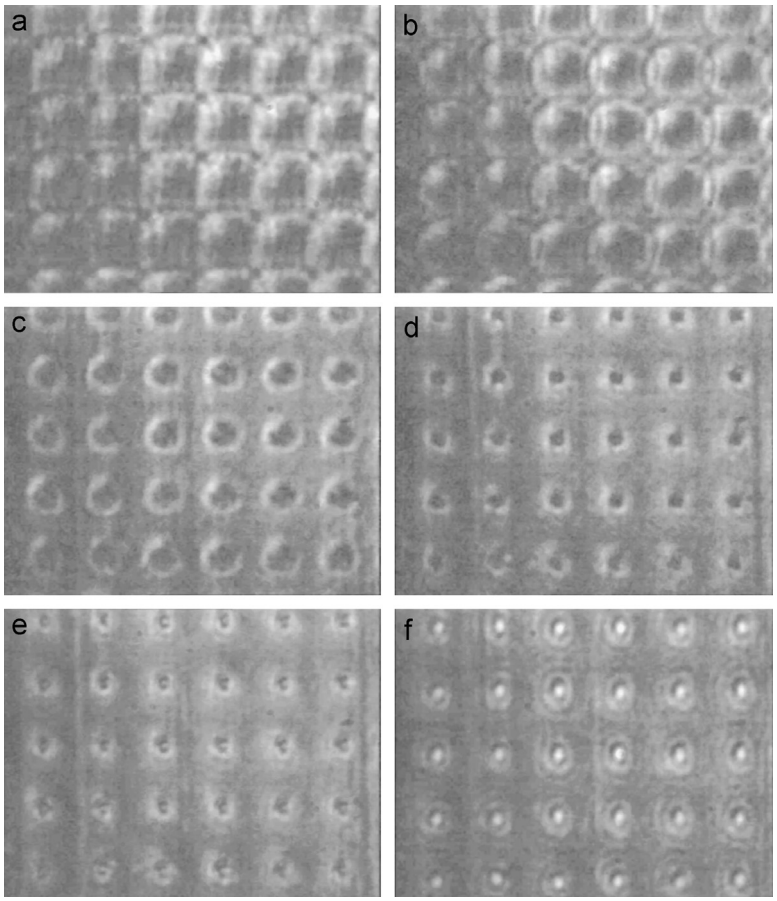

Fig. 3. Optical phenomena exhibited by the C-MLA device at 0.106 V/μm as the device is moved along the optic axis z. [*Lenslet spacing*=10 μm.] (a) $z=0$ μm, (b) $z=-8$ μm, (c) $z=-28$ μm, (d) $z=-41$ μm, (e) $z=-48$ μm and (f) $z=-69$ μm.

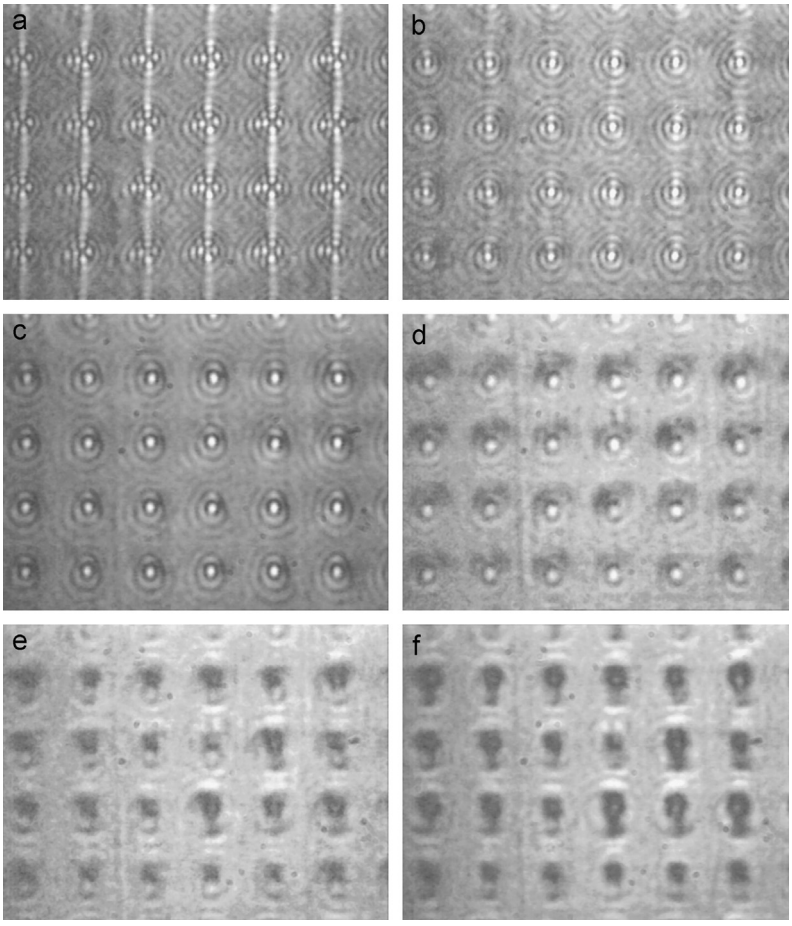

Fig. 4. Typical optical phenomena exhibited by the C-MLA device at different high frequency ac voltages for a fixed location along the optic axis. [*E-field frequency* = 1.1 kHz; *lenslet spacing* = 10 μm.] (a) 0.000 V/μm, (b) 0.060 V/μm, (c) 0.074 V/μm, (d) 0.134 V/μm, (e) 0.177 V/μm and (f) 0.237 V/μm.

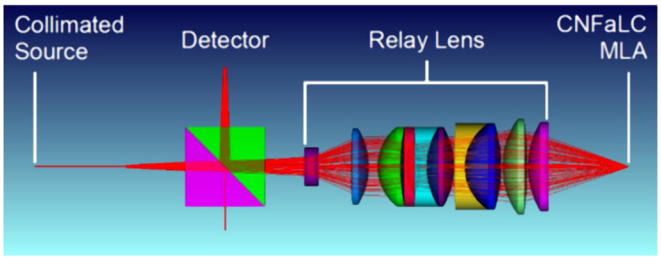

Fig. 5. Zemax model for the experimental setup.

There has already been some success reported for characterizing the C-MLA device by looking at its phase profile [5,9,12–14]. Indeed this is a typical approach for LC lenses [15–18]. However these results, whilst useful for giving a broad understanding of the C-MLA device, are not specific enough for use in optical design applications. Unlike the work presented here, their analysis methods do not take into account what impact the imaging system might have. For example in each case polarized microscopy is used where the imaging beam at the C-MLA is not collimated. Furthermore, these studies use a singular optical profile taken at a chosen plane to discern the optical properties of a C-MLA lenslet, often assuming a fixed lens diameter of 5 μm [5,12,14,19]. While this may be valid for simple 2D planar lenses, a C-MLA lenslet is far more complex. Indeed the *E*-field models suggest a lens diameter and a phase profile that varies non-trivially along the optic axis. This paper will show that our results are more in concordance with the work conducted by Butt et al. [9].

1.1. C-MLA device structure

A basic schematic of the C-MLA device is shown in Fig. 1.[3] At its base was a vertically aligned CNF array. Each C-MLA lenslet was spaced 10 μm apart and at the center of each was a group of four CNFs of typically 50 nm diameter spaced 1 μm apart. Each group of four was arranged in a square pattern and was spaced 10 μm apart.

The base of the device was magnetron-sputtered with a 400 nm layer of Aluminum, making it highly reflective and conductive. This acted as a common electrode connecting the CNF array to an ac voltage supply. A 0.5 mm ITO-coated borosilicate glass was used as a grounded top electrode. Its underside was coated with an alignment layer (AM4276, Merck) rubbed horizontally to planar align the LC. There was a 20 μm gap between the top and bottom electrodes which was filled in a vacuum with a nematic LC (BL048, Merck).

When ac voltage was applied across the C-MLA the CNFs acted as field enhancers. A Gaussian-like *E*-field was formed above each central group of four CNFs [9,19] and reorientated the dielectrically anisotropic LC molecules. Since the LC was optically birefringent, this set up a region of tunable gradient refractive index that acted as an adaptive optical element with lens-like properties.

Specifically, any extraordinary rays were affected by the LC molecular orientation. Under lensing conditions these rays reflected back from the Al backplane to form a wide-angle beam. The ordinary

[3] The pertinent aspects of the C-MLA device are presented here for reference. Details of the manufacturing process can be found in [1].

rays and any extraordinary rays outside the lensing area would reflect back at a much narrower beam angle. The observed optical phenomena were therefore also the resulting interference patterns.

2. Experiments

2.1. Imaging setup

Previous work suggested that C-MLAs have very short focal lengths of 7–15 μm which would make the focal plane somewhere within the device [5,13,14]. This, in addition to the size and reflective nature of the C-MLA device, necessitated an imaging lens to relay any optical phenomena of interest to the detector. We used an Edmund Optics (EO) objective lens (20× EO M Plan Apo Long Working Distance Infinity-Corrected, #59-878).

The experimental layout is shown in Fig. 2. The imaging source was a 35 mW, 658 nm fiber laser (LPS-660-FC, Thorlabs) with linearly polarized light as output. This imaging beam was collimated and tuned with a $\lambda/2$-waveplate before passing through a polarizing beamsplitter (PBS) cube. After reflecting off a mirror and passing through a second BS it was focused at the C-MLA by the EO objective lens. The resulting interference pattern was relayed back by the EO objective to the detector via the second BS.[4]

2.2. Experimental results

Some optical phenomena of note of the C-MLA are shown in Fig. 3. Images were recorded as the C-MLA was moved along the optic axis to reveal what was happening in the image space of the lens array. A typical set of results is shown in Fig. 3 for 0.106 V/μm. These are the first reported images of the intensity profile variation along the optic axis for the C-MLA.

A key advantage of the C-MLA over conventional microlens arrays is its adaptability; its optical properties can be tuned using the externally controlled *E*-field. Fig. 4 shows some of the typical phenomena observed as different field strengths were applied across the C-MLA device. The C-MLA was tested up to 0.276 V/μm to avoid damaging the device.

The optical properties and behavior of the C-MLA are clearly complex. Changes in the recorded intensity distribution appeared from as low as 0.014 V/μm as the LC molecules began to reorient to the *E*-field. However the C-MLA began to exhibit properties comparable to those of classical MLAs from around 0.060 V/μm. In this *lensing mode* a distinct high intensity central focal spot could be obtained within a number of circular concentric fringes (e.g. Fig. 4(b)–(d)). When the *E*-field was increased from 0.060 V/μm to 0.276 V/μm the number of visible fringes decreased but the minimum focal spot size increased. It was in this range that the C-MLA device could be considered to be acting as an MLA.

The best quality C-MLA with the least fringes and smallest focal spots was achieved at 0.106 V/μm. The focal plane shown in Fig. 3 (e) shows that the C-MLA has true potential as an adaptive substitute for classic MLAs in most optical systems.

3. Simulations

The approach presented here uses Zemax to model the experimental system in its entirety. Optical models of the C-MLA were devised and input into the system to try and reproduce the experimental results. In this way, we have developed the first optical models of the C-MLA.

[4] This particular configuration with a double-pass through the EO objective was necessary to preserve the optical properties of both the objective and C-MLA, thus achieving the best image quality possible. The additional PBS built into the experimental setup allowed a secondary reference beam to be generated when necessary for testing purposes but was not used for the results published here.

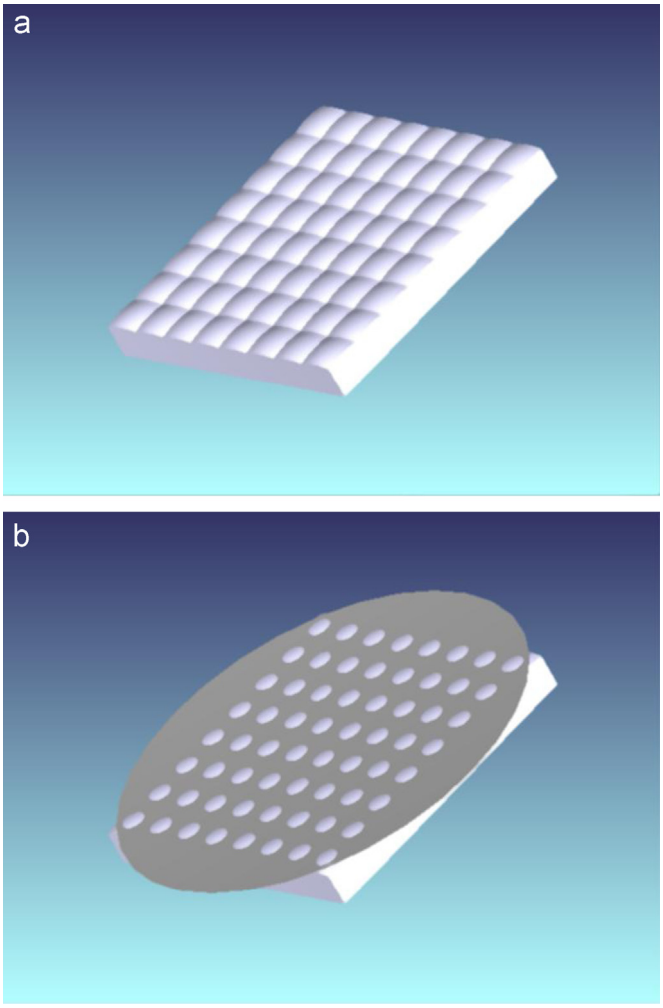

Fig. 6. Model for the C-MLA; MLA pitch = 10 μm; front surfaces are reflective. (a) Plano-convex square MLA and (b) intersecting with a reflective plane.

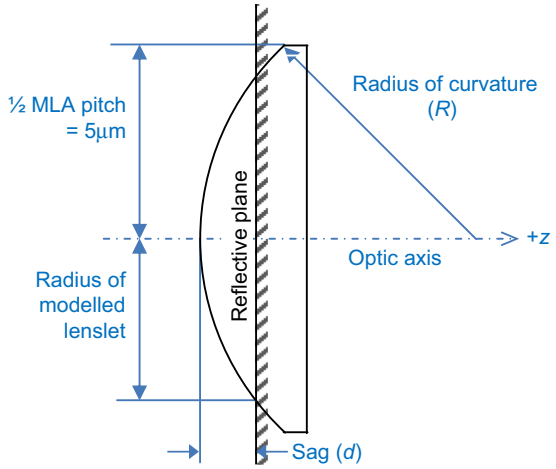

Fig. 7. Parameters used to define the modeled lenslets.

3.1. Model of setup

Fig. 5 shows the Zemax model of the experimental setup. The optical specification of the EO objective lens was unavailable so

one of similar size and near-identical optical properties was designed to ensure an accurate simulation and an authentic C-MLA model. In particular, both objective lenses have an effective focal length (EFL) of 10 mm, a numerical aperture (NA) of 0.4 and can achieve a resolution of 0.7 μm.

3.2. Models of the C-MLA

This study focused on modeling the C-MLA device in its lensing mode. In this case, with the aim of using the device as a substitute for classical MLAs, the most critical set of results was that for 0.106 V/μm since it produced the smallest and most efficient array of focal spots. Indeed the intensity distribution in the image space of the C-MLA at 0.060–0.276 V/μm was simple variations of that shown for 0.106 V/μm in Fig. 3, as indicated in Fig. 4.

While the exact graded refractive index profile for the C-MLA is unknown, the LC has positive dielectric anisotropy and birefringence so should form negative lenses [9]. The discrete intensity patterns suggested a discrete lens array. This can be represented as an array of negative microlenses with a mirrored backplane.

Various models were developed to try and reproduce the experimental results. It was found that most of the properties exhibited in stronger *E*-fields could be reproduced using a simple reflective convex square lens array intersecting with a flat reflective plane. This created an array of circular diverging optical elements with a mirrored backplane, as shown in Fig. 6. The exact profile of the lens array could be adjusted and the location of the intersecting reflective plane could be used to adjust both the lenslet sag *d* and its modeled radius or aperture (see Fig. 7).

4. Results and discussion

Fig. 8 shows the simulation results matched to the 0.106 V/μm experimental results. In this instance the simulation incorporated a model MLA with a radius of curvature of 30 μm. This equates to an EFL of 15 μm for a spherical lens. The sag *d* and conic constant *k* were then used to modify the C-MLA model where necessary.

In particular, the experimental results showed that the central area of low intensity that appeared in front of the imaged focal plane decreased as we approached the focal plane (see Fig. 8(b)–(d)). This region of low intensity was likely due to the divergent nature of the C-MLA lenslets. The bright fringe visible around it is from interference between the divergent beam of the negative lens and the light reflected from the backplane. This was simulated by reducing the sag, which in turn reduced the aperture of the modeled lenslets. This suggested that the aperture of the true C-MLA lenslets could vary along the optic axis, which would concur with the *E*-field models presented by Butt et al. in 2011 [9].

While the spherical lenslet model produced results with good congruence with the experimental results on the most part, a low order aspheric lenslet model was necessary to reproduce the results from the focal plane onwards. Spherical lenses produced

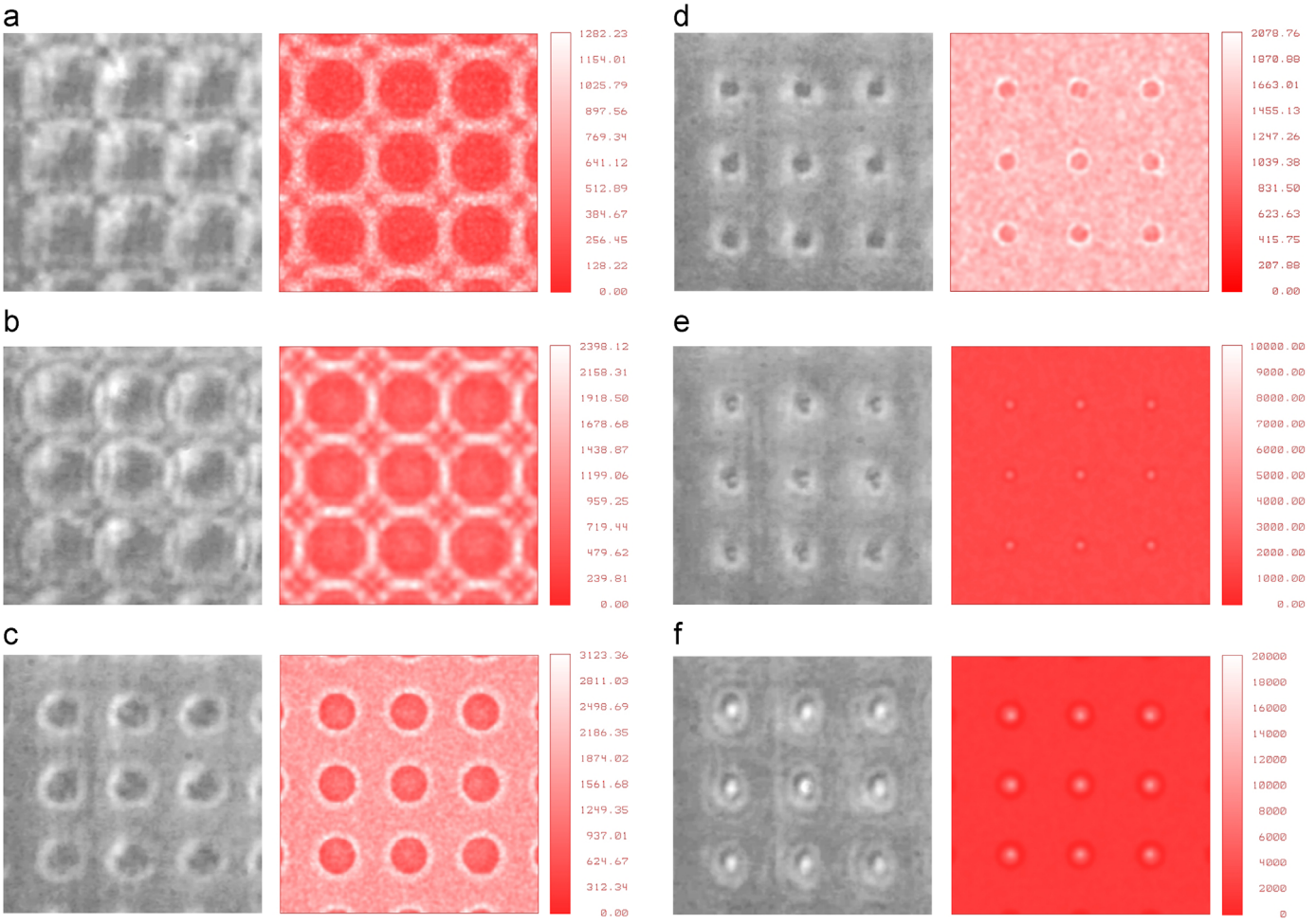

Fig. 8. Experimental (*upper*) and simulated (*lower*) coherent irradiance results for the C-MLA along the optic axis at 0.106 V/μm using a C-MLA model with radius of curvature $R=30$ μm. [*d=sag*; *k=conic constant.*] (a) $d=0.2678$ μm, $k=0$; (b) $d=0.2678$ μm, $k=0$; (c) $d=0.1300$ μm, $k=0$; (d) $d=0.0400$ μm, $k=0$; (e) $d=0.0168$ μm, $k=10$; (f) $d=0.0700$ μm, $k=-100$.

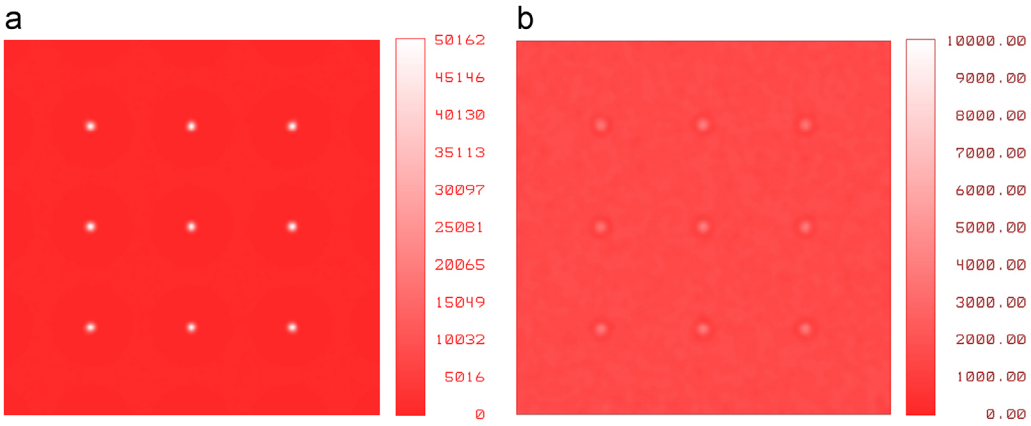

Fig. 9. Effect of varying conic constant at the focal plane: (a) $k=0$ and (b) $k=10$.

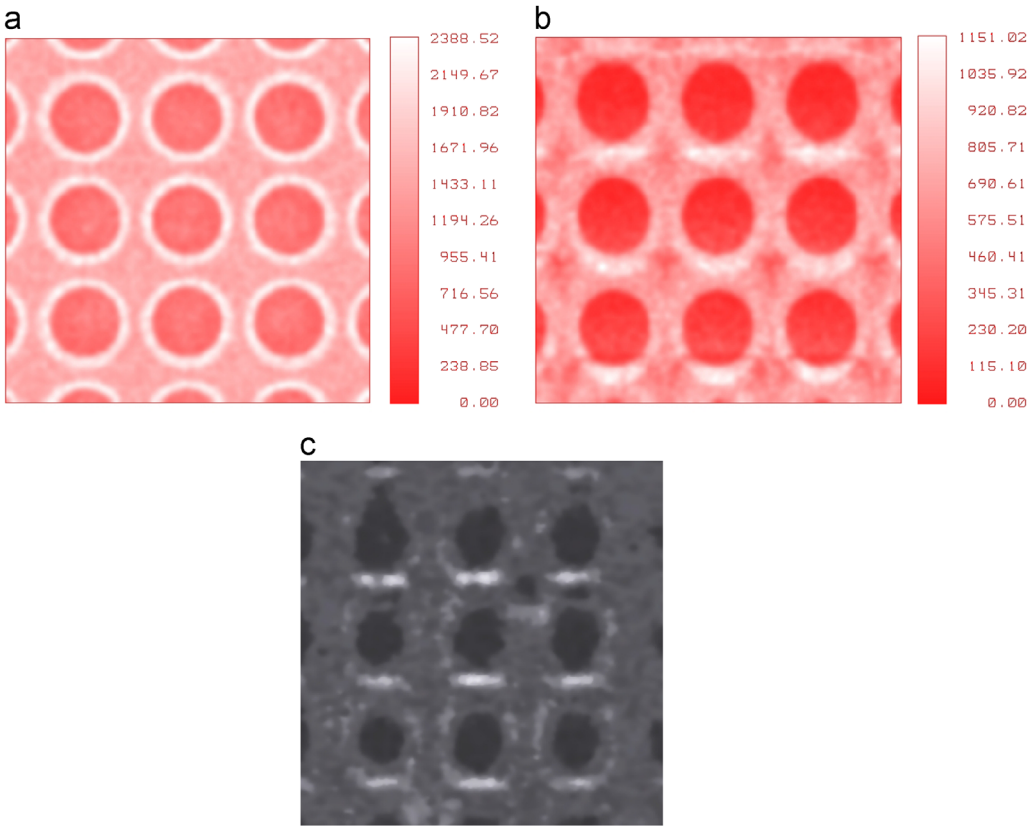

Fig. 10. Simulated coherent irradiance for a C-MLA model with $R=20$ μm, $k=-0.6$, $d=0.15$ μm (a) without tilt and (b) tilted by 10° about the x-axis. (c) Experimental result taken at 0.276 V/μm for comparison.

very sharp focal points (see Fig. 9). However Fig. 8(e) shows the minimum spot size for the C-MLA is significantly larger. This means there must be significant aberration in the C-MLA. We reproduced this by varying the conic constant which reproduced the larger central region of high intensity well (see Fig. 8 (e) and (f)).

4.1. Tilt

The simulations showed that the C-MLA lenses appeared to be tilted with respect to the surface normal. This is shown more clearly in Fig. 10(c), where it appears as an asymmetry in the recorded intensity pattern.

The tilt exhibited in the experiments was relatively small and was likely due to either the alignment layer causing a certain degree of tilt to the 3D lens structure throughout the device or the non-telecentricity of the EO relay lens. Testing the C-MLA experimentally with a telecentric relay lens would be the only way to distinguish between the two and is currently being investigated.

4.2. Multiple fringes

The C-MLA behaved mostly like a simple classical optical element. This was a key result as it showed that the C-MLA can successfully substitute for classical MLAs when this relay setup is used. However there is an interesting discrepancy. The simulation result in Fig. 8(f) was achieved by adjusting the conic constant to increase the size of the central high intensity region. However more fringes are visible in Fig. 8(f) and significantly more are shown in Fig. 4(a) and (b).

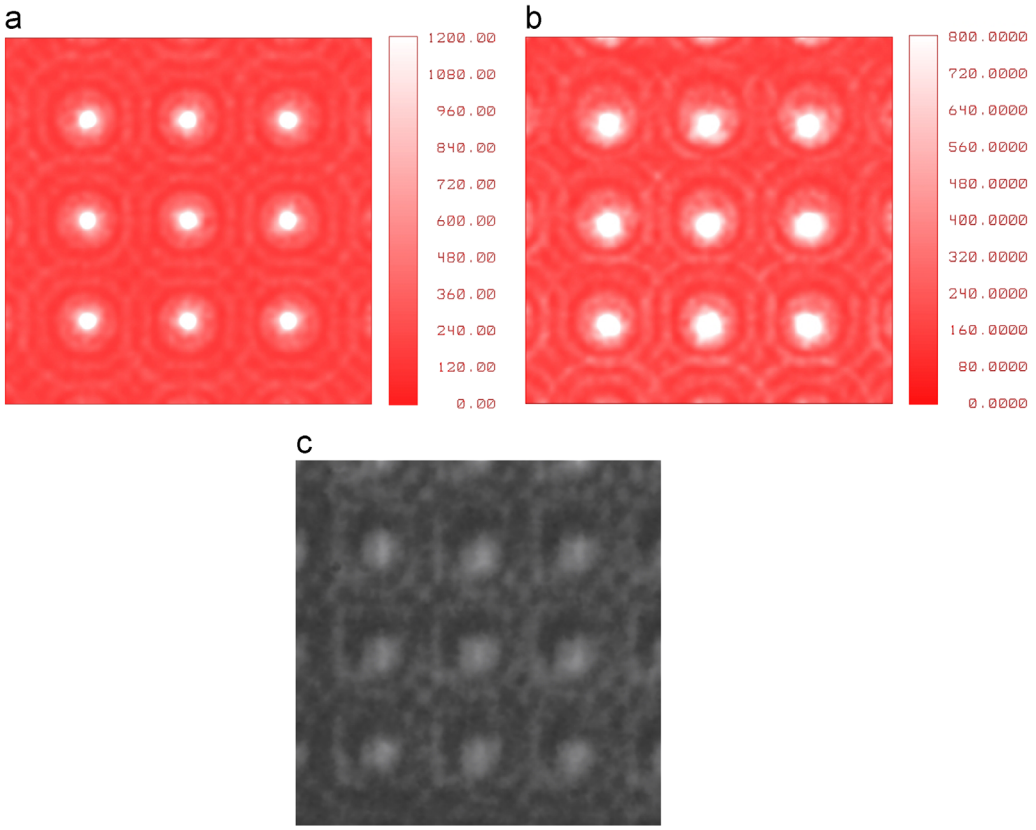

Fig. 11. (a) Multiple fringes obtained using a high power aspheric lens with radius of curvature $R=10$ μm, conic constant $k=-5$ and sag $d=0.02678$ μm. (b) Simulation result with 2° tilt about x-axis. (c) Experimental result taken at 0.141 V/μm.

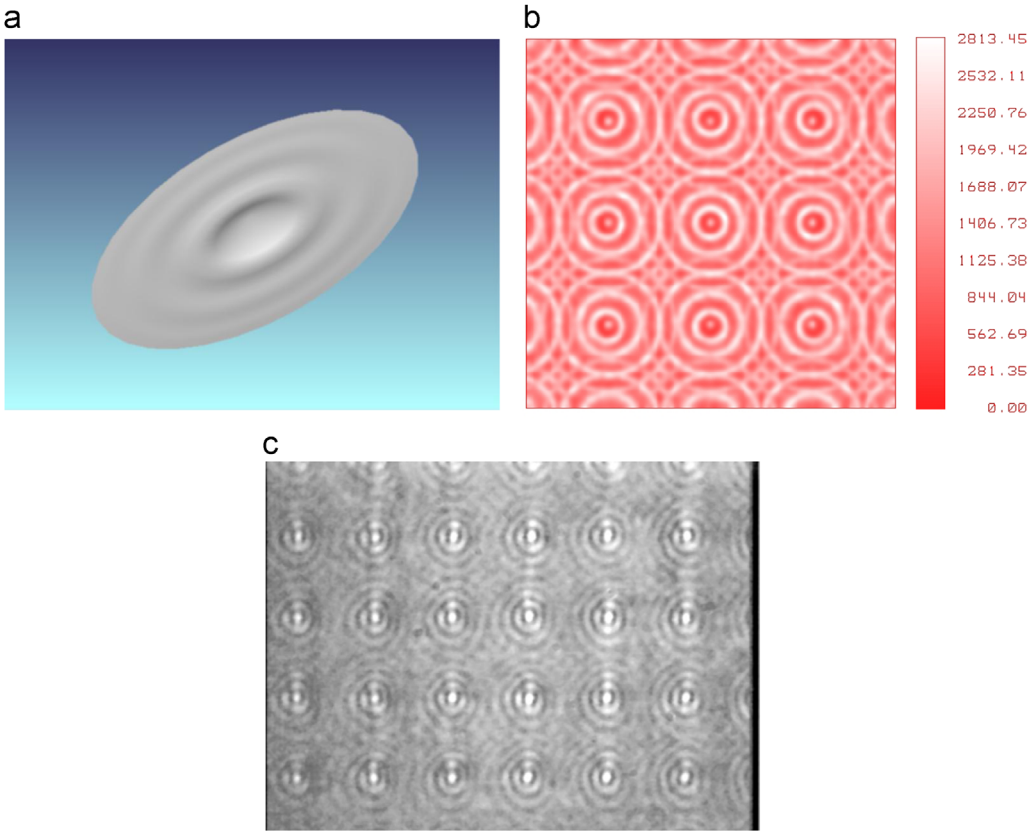

Fig. 12. Multiple fringes obtained using a Gaussian-like lens with side lobes. Central lobe radius=4 μm; surface radius=7 μm. (a) Lens profile. (b) Simulation result and (c) Experimental result.

Table 1
Zemax lens data for a Gaussian-like lens with side lobes.

Radius of curvature (R)	1.4860705×10^{-3}
Conic constant (k)	$-9.5983217 \times 10^{-1}$
r^2	-2.1751282×10^{2}
r^4	-3.1684151×10^{7}
r^6	3.7105844×10^{12}
r^8	$-2.5301183 \times 10^{17}$
r^{10}	9.9058247×10^{21}
r^{12}	$-2.2323672 \times 10^{26}$
r^{14}	2.6851237×10^{30}
r^{16}	$-1.3397845 \times 10^{34}$

A simple solution to increasing the number of visible fringes was to increase the aberration in the MLA model or the power of the lens. This is shown in Fig. 11 with a high power aspheric C-MLA model. This would again concur with the predicted *E*-field distributions [9], which suggests that the *E*-field is stronger and more concentrated at the CNF tip, thus resulting in a higher power lens with reduced aperture. However there is a limit to this method. Given the numerical aperture of the relay lens, NA=0.4, the source wavelength, $\lambda = 658$ nm, the pitch of the MLA, $p = 10\ \mu$m and taking into account the reflective nature of the C-MLA, the maximum number of fringes that could be achieved with a lens and a planar reference beam would be 3.17 fringe pairs.

Fig. 4 clearly shows that there were the instances where more than 3.17 pairs were imaged. In these cases there must have been a non-planar beam interfering with another non-planar beam. This was possible if the refractive lens structure or physical CNF array was causing a disturbance in the surrounding LC outside the main lensing area [1]. Fig. 12 shows the effect which even a very minor "rippled lens" may cause. Here a Gaussian-like lens was used with ripples of less than 1/20th of the amplitude of the main lobe. Table 1 gives the Zemax lens data used to generate this model.

To the best of our knowledge this is the first reported evidence of this phenomenon. It is likely that the multiple fringes seen were a combination of both these factors, especially since more numerous fringes appeared at low *E*-field strengths where the defects in the LC texture caused by the CNF array would dominate.

5. Conclusions and future work

In summary, this paper presented the first images of the optical profile for the C-MLA along the optic axis. We also presented a novel method of reverse-engineering the first working optical models of the C-MLA using Zemax. This approach bypassed the need to know the exact CNF–LC interaction and can be easily adapted to other systems where the nature of an optical device is unknown.

The results presented here shows that the C-MLA behaves like a simple lensing system at 0.060–0.276 V/μm. In this lensing mode the C-MLA could be modeled as a reflective convex lens array intersecting with a flat reflective plane. Specifically, our results indicated that the C-MLA exhibited characteristics of mostly spherical or low order aspheric lens arrays in strong *E*-fields, with some aspects of high power aspherics. The C-MLA has been also shown to exhibit properties associated with varying lens apertures and powers, which concur with previous theorized lens models based on *E*-field patterns. We uniquely provided evidence demonstrating an apparent "rippling" of the LC texture in weak *E*-fields, most likely due to defects caused by the CNF array. These were successfully reproduced using rippled Gaussian-like lens profiles.

This approach produced simulation results that matched well with experimental results. It has proven to be a promising and useful method of characterizing the C-MLA and planned future work includes developing lensing models with varying or graded refractive index models. This could provide more specific information on actual LC distribution.

Acknowledgments

This work is supported by the Engineering and Physical Sciences Research Council (EPSRC). Jiahui Lu wishes to acknowledge Dr. Haider Butt for the many fruitful discussions.

References

[1] T.D. Wilkinson, X. Wang, K.B. Teo, W.I. Milne, Adv. Mater. 20 (2) (2007) 363.
[2] H. Lin, M. Chen, Y. Lin, Trans. Electr. Electron. Mater. 12 (2011) 234.
[3] H.S. Jeong, S.C. Youn, Y.H. Kim, H.-T. Jung, Phys. Chem. Chem. Phys. 15 (2013) 9493.
[4] E. Sen, N. Kaya, A. Alicilar, J. Mol. Liq. 186 (2013) 33.
[5] R. Rajasekharan-Unnithan, H. Butt, T.D. Wilkinson, Opt. Lett. 34 (8) (2009) 1237.
[6] J. Lagerwall, G. Scalia, J. Mater. Chem. 18 (25) (2008) 2890.
[7] I. Baik, S. Jeon, S. Jeong, S. Lee, K. An, S. Jeong, Y. Lee, J. Appl. Phys. 100 (2006) 074306.
[8] S. Jeong, P. Sureshkumar, K. Jeong, A. Srivastava, S. Lee, S. Jeong, Y. Lee, R. Lu, S. Wu, Opt. Express 15 (2007) 11698.
[9] H. Butt, R. Rajasekharan, T.D. Wilkinson, G.A. Amaratunga, IEEE Trans. Nanotechnol. 10 (3) (2011) 547.
[10] Zemax EE Optical Design Program, Zemax Development Corporation, Redmond, WA, USA, May 2009.
[11] Radiant Zemax LLC, August 2013, www.radiantzemax.com/zemax.
[12] R. Rajasekharan, Q. Dai, H. Butt, K. Won, T.D. Wilkinson, G.A. Amaratunga, Appl. Opt. 51 (4) (2012) 422.
[13] X. Wang, T.D. Wilkinson, M. Mann, K.B. Teo, W.I. Milne, Appl. Opt. 49 (17) (2010) 3311.
[14] R. Rajasekharan, Q. Dai, T.D. Wilkinson, Appl. Opt. 49 (11) (2010) 2099.
[15] D. Liang, Q.-H. Wang, J. Disp. Technol. PP (99) (2013) 1.
[16] M. Ye, B. Wang, S. Sato, Opt. Commun. 259 (2) (2006) 710.
[17] M. Ye, S. Sato, Opt. Commun. 225 (4–6) (2003) 277.
[18] Y. Takaki, H. Ohzu, Opt. Commun. 126 (1–3) (1996) 123.
[19] Q. Dai, R. Rajasekharan, H. Butt, K. Won, X. Wang, T.D. Wilkinson, G. Amaragtunga, Nanotechnology 22 (11) (2011) 115.